Liquid thermoelectric conversion devices composed of several organic solvents

Akihiro Wake[1], Dai Inoue[1], and Yutaka Moritomo[1,2,3]*

[1] *Graduate School of Pure & Applied Science, University of Tsukuba, Tennodai 1-1-1, Tsukuba, Ibaraki 305-8571, Japan*

[2] *Faculty of Pure & Applied Science, University of Tsukuba, Tennodai 1-1-1, Tsukuba, Ibaraki 305-8571, Japan*

[3] *Tsukuba Research Center for Energy Materials Science (TREMS), University of Tsukuba, Tennodai 1-1-1, Tsukuba, Ibaraki 305-8571, Japan*

We evaluated the performances of liquid thermoelectric conversion devices (LTEs) composed of nine organic solvents containing Fe^{2+}/Fe^{3+} redox pair against electrolyte concentration (m). In protic solvents, *i.e.*, methanol (Me), ethanol, (Et) 1-propanol (Pr), and ethylene glycol (EG), the electrochemical Seebeck coefficients ($\alpha = dV/dT$; where V and T are the electrode potential and temperature, respectively.) increases with m in small m region. Based on the ultra violet - visible (UV-vis) absorption spectroscopy, we interpreted the enhancement of α in terms of the OH^- and/or H_2O coordination to Fe^{3+}, which was introduced by crystal water of the solute. At the temperature difference (ΔT) of 30 K, the maximum value (PF_{max}) of the power factor (PF) of the Me LTE reaches 11.5 $\mu W/K^2m$.

1. Introduction

Energy harvesting devices that produces electric energy from small environmental energy, such as thermal flow and temperature, is indispensable for realizing the IoT (Internet of Things) society, because the device is a permanent power source and does not require replacement or maintenance. Among the energy harvesting devices, liquid thermoelectric conversion device (LTE) with very simple and low-cost structure is attracting attention. The LTE consists of the electrolyte solution with a redox couple and hot/cold electrodes of identical type. The LTE was proposed in the 1950s and is still undergoing focused exploration and development.[1–31] Like a solid thermoelectric conversion device (STE),[32] the device converts temperature difference (ΔT) between the electrodes to thermal voltage ($V = \alpha \Delta T$) via the electrochemical Seebeck coefficient ($\alpha \equiv \frac{dV}{dT}$, where V and T are the redox potential and temperature, respectively.). The essential parameters that determine performance of LTE are α, electrical conductivity (σ), and thermal conductivity (κ) of the electrolyte solution. The performance indicators of

*E-mail: moritomo.yutaka.gf@u.tsukuba.ac.jp

thermal conversion, *i.e.*, the dimensionless figure of merit (ZT) and power factor (PF), are expressed as $ZT = \frac{\alpha^2 \sigma T}{\kappa}$ and $PF = \alpha^2 \sigma$.

Until now, LTE research and development have been focused on aqueous solution that easily dissolves electrolyte. In aqueous solution containing Fe^{2+}/Fe^{3+} redox pair, the α value significantly depends on the counter anion and pH and ranges from 0.18 mV/K for $(NH_4)FeSO_4/(NH_4)_2FeSO_4$[33] to 1.76 mV/K for $Fe(ClO_4)_2/Fe(ClO_4)_3$.[34] Recently, Inoue *et al.*[35] systematically investigated the α values of Fe^{2+}/Fe^{3+} redox pair dissolved in organic solvents and found that the α values in several aprotic solvents are extremely high. For example, α in acetone and acetonitrile (AN) containing 10 mM $FeCl_3$ and 10 mM $FeCl_2$ is 3.60 mV/K and 2.16 mV/K, respectively. Wake *et al.*[1] fabricated LTEs composed of water, acetone and AN containing $Fe(ClO_4)_2/Fe(ClO_4)_3$ and evaluated their performances against electrolyte concentration (m). At ΔT = 30 K, the maximum value (ZT_{max}) of ZT of the acetone LTE reaches 0.0164 at m = 0.5 M and that of the AN LTE reaches 0.0144 at 0.5 M.[1] These values are larger than ZT_{max} (= 0.0116 at 0.5 M) of the corresponding aqueous LTE.

In this paper, we evaluated the performances of LTEs composed of nine organic solvent containing m M $Fe(ClO_4)_2 \cdot 6H_2O$ and m M $Fe(ClO_4)_3 \cdot 7.1H_2O$ against m. In protic solvents, *i.e.*, methanol (Me), ethanol (Et), 1-propanol (Pr), and ethylene glycol (EG), the α value increases with m in small m region. At ΔT of 30 K, the maximum value (PF_{max}) of the power factor (PF) of the Me LTE reaches 11.5 $\mu W/K^2m$. In protic solvents, the α value increase with m in small m region due to the crystal water in the solute. The enhancement of α is interpreted in terms of the heterologous coordination to the Fe ion.

2. Experimental method

2.1 Solution preparation

The solvents investigated were Me (FUJIFILM Wako corp.), Et (FUJIFILM Wako corp.), Pr (FUJIFILM Wako corp.), EG (FUJIFILM Wako corp.), tetrahydrofuran (THF; FUJIFILM Wako corp.), propylene carbonate (PC; FUJIFILM Wako corp), N,N-dimethylformamide (DMF; FUJIFILM Wako corp.), dimethyl sulfoxide (DMSO; FUJIFILM Wako corp.), and N-methyl pyrrolidone (NMP; FUJIFILM Wako corp.). The solvents are purchased and used as received. The solutions contains m M $Fe(ClO_4)_2 \cdot 6H_2O$ (FUJIFILM Wako corp.) and m M $Fe(ClO_4)_3 \cdot 7.1H_2O$ (FUJIFILM Wako corp.). We did not perform dehydration process and solution contains some water. Unfortunately, the maximum value (m_{max}) of m is very small in several aprotic solvents; $m_{max} \approx 0.3$ M in DMF, ≈ 0.1 M in DMSO, and ≈ 0.1 M in NMP.

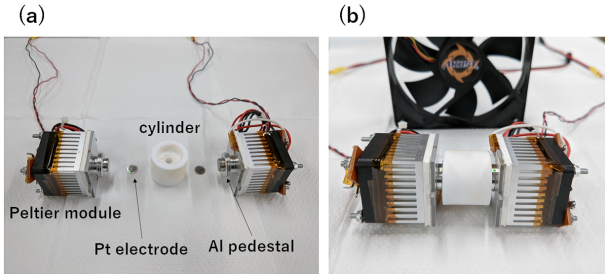

Fig. 1. (Color online) Pictures of thermocell in (a) disassembled and (b) assembled states.

2.2 Thermocell

The LTE performance was evaluated with use of a specially-designed thermocell.[36] Figure. 1 show pictures of the thermocell in (a) disassembled and (b) assembled states. The electrolyte was filled in a 0.73 mmϕ polytetrafluoroethylen (PTFE) cylinder. Both ends were sealed with the Al pedestals, on which Pt disks with an area (S) of 0.42cm^2 were attached as hot and cold electrodes. The two Pt electrodes were placed at a distance (D) of 1.0 cm. The temperatures of hot ($T_{\rm hot}$) and cold ($T_{\rm cold}$) electrodes are independently controlled with Peltier modules. $T_{\rm hot}$ and $T_{\rm cold}$ were monitored with T-type thermocouples, which were attached at the Al pedestals at 2 mm from the Pt electrodes.

We note that the σ value of an operating LTE depends on the cell size and shape, *i.e.*, S and D, reflecting the convection, concentration overpotential, wall effect, and so on.[37] Especially, the σ value during the LTE operation significantly suppressed at small D, especially below 0.5 cm.[38] To quantitatively compare the LTE performances, the physical quantities should be evaluated with the same cell size and shape. The S (= 0.42 cm^2) and D (= 1.0 cm) values in the present investigation is the same as those in the previous report.[1]

2.3 ΔT - V_0 plot

To determine α, the open circuit voltage (V_0) was measured against ΔT (= $T_{\rm hot}$ - $T_{\rm cold}$) with fixing $T_{\rm cold}$ at 298.3 K. $T_{\rm hot}$ was manually controlled by changing stepwise the current flowing through the Peltier device at intervals of 5 minutes. The V_0 values were measured under steady state with use of digital multimeter (Keithley 2100; Tektronics). We confirmed that the ΔT - V_0 plots in the ΔT-increasing and ΔT-decreasing runs were almost overlapped with each other. α was evaluated as the slope of the ΔT - V_0 plot.

2.4 I - V plot

We further investigated voltage (V) against current density (I) during the LTE operation at a fixed ΔT (= 30 K). T_{hot} and T_{cold} were set to be 298.3 K and 328.3 K, respectively. The I value was controlled by an external resistance (R_{ex}). The V values on the external resistor were measured under steady state with use of digital multimeter (Keithley 2100; Tektronics). The I (= $\frac{V}{R_{\mathrm{ex}}}$) values were evaluated from V and R_{ex}. If we assume an internal resistance (R_{in} = $\frac{D}{\sigma}$), V is expressed as $V = V_0 - \frac{D}{\sigma}I$. The effective σ values in an operating LTE device was evaluated from the slope of the the I - V plot. We note that thus evaluated σ includes the effects of the convection and temperature gradients. In this work, we intended to determine the actual σ in an operating LTE device. On the other hand, the power density ($P = IV$) of is expressed as $P = -\frac{D}{\sigma}I^2 + V_0 I$. P becomes maximum ($P_{\mathrm{max}} = \frac{\sigma V_0^2}{4D} = \frac{\alpha^2 \sigma \Delta T^2}{4D}$) at $I = \frac{\sigma V_0}{2D}$. The coefficient, $\alpha^2\sigma$, of P_{max} is called as power factor (PF).

3. Results and discussion

3.1 ΔT - V_0 plot

Figure 2 shows V_0 - ΔT plots of LTEs composed of (a) Me, (b) Et, (c) Pr, (d) EG, (e) THF, (f) PC, (g) DMF, and (h) DMSO containing m M $Fe(ClO_4)_2 \cdot 6H_2O$ and m M $Fe(ClO_4)_3 \cdot 7.1H_2O$. Straight lines are results of least-squares fitting. The slope corresponds to respective α. In (a) Me, the α value significantly increases with m from 1.18 mV/K at 0.1 M to 1.85 mV/K at 0.5 M. Above m = 0.5 M, the α value gradually decreases with m to 1.52 mV/K at 1.0 M. Similar enhancement of α is observed in the other protic solvent, *i.e.* (b) Et, (c) Pr and (d) EG. The enhancement of α is originated in the crystal water of the solute (*vide infra*). In (e) THF, the α value monotonously decreases with m from 3.16 mV/K at 0.1 M to 2.10 mV/K at 0.5 M. A similar monotonous decrease of α is observed in the other aprotic solvent, *i.e.* (f) PC, (g) DMF, and (h) DMSO

Figure 3 shows the α values in (a) protic and (b) aprotic solvents against m. In (a) protic solvents, α increases with m in small m region and decreases with m in large m region, as indicated by solid curves. In (b) aprotic solvents, α monotonously decreases with m, as indicated by broken straight lines. A similar decrease of α with m is reported in the other aprotic solvents, such as acetone and AN.[1)]

We note that the α values in aprotic THF and PC are much higher than the α values of protic solvents. In a thermodynamical point of view, α is equivalent to $\frac{\Delta S}{e}$, where e and ΔS are the elementary charge (≥ 0) and variation in the system entropy (S) in the reduction process. In solute-solvent system, ΔS is dominated by the configuration entropy of the solvent

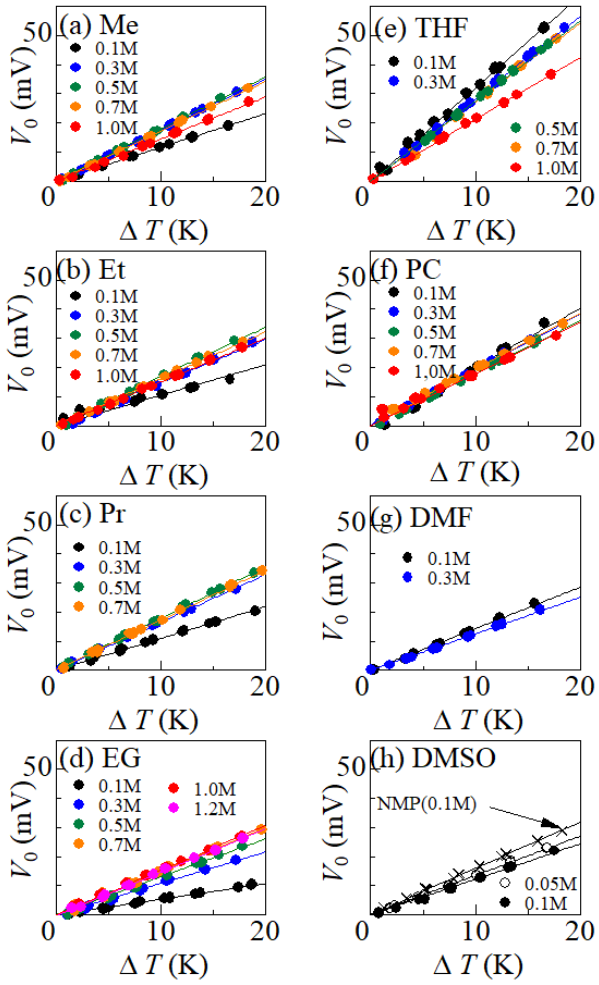

Fig. 2. (Color online) Open circuit voltage (V_0) against temperature difference (ΔT) between hot and cold electrodes in LTEs composed of (a) methanol (Me), (b) ethanol (Et), (c) 1-propanol (Pr) , (d) ethylene glycol (EG), (e) tetrahydrofuran (THF), (f) propylene carbonate (PC), (g) N,N-dimethylformamide (DMF), and (h) dimethyl sulfoxide (DMSO) containing m M $Fe(ClO_4)_2{\cdot}6H_2O$ and m M $Fe(ClO_4)_3{\cdot}7.1H_2O$. NMP stands for N-methyl pyrrolidone. Straight lines are results of least-squares fitting.

molecules surrounding the solute ion.[35] In an aprotic solution where interaction between the solute ion and solvent molecule is weak, the coulombic potential of the solute ion influences the configuration of the solvent molecules even in the second nearest-neighbor region. Then, the reduction process of the central Fe ion has more significant effect on the configuration entropy of the solvent molecules. This situation explains the higher α values observed in aprotic THF and PC.

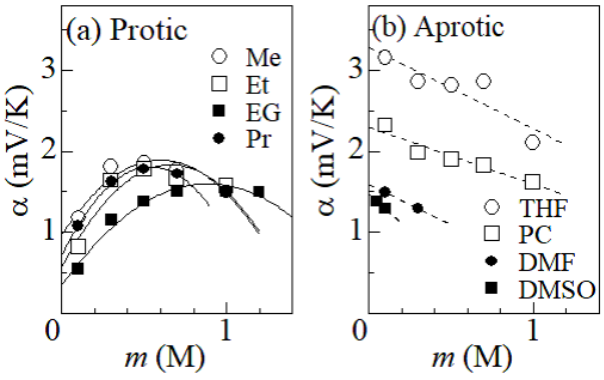

Fig. 3. Electrochemical Seebeck coefficient (α) of Fe^{2+}/Fe^{3+} redox pair dissolved in (a) protic and (b) aprotic solvents against electrolyte concentration (m). Solid curves in (a) are results of least-squares fitting with quadratic functions. Broken straight lines in (b) are results of least-squares fitting.

3.2 Decrease of α with m

In aprotic solvents, α shows monotonous decrease with m, as indicated by broken straight lines in Fig. 3(b). A similar decrease is discernible in protic solvents, as indicated by solid curves in Fig. 3(a). The suppressed α in dense solvents can be ascribed to the interaction between the neighboring Fe ions.

The Fe ions in solution are coordinated and/or surrounded by solvent molecules, as schematically shown in Fig. 4(a). A large circles represent the interaction area where solvent molecules interact electrostatically and/or quantum mechanically with the central Fe ion.[39] The reduction process of the central Fe ion increases the configuration entropy of the solvent molecules because decease of the Fe valence reduces the Coulomb interaction between Fe ion and the polar ligand molecules. Tha change in the configuration entropy is the main origin for ΔS in a solute-solvent system.[35] The interaction areas of individual Fe ions are well isolated in dilute solution. In dense solution, a part of the interaction area overlaps with the neighboring areas, as indicated by hatchings in Fig. 4(b). Actually, the number of solvent molecules per one Fe ion is 6.1 (5.8) in THF (PC) at m = 1.0 M. The overlapping area, and hence, the number of the solvent molecules in the overlapping region, increases with increase in m. The solvent molecule in the overlapping region interacts with multiple Fe ions, and hence, is less sensitive to the reduction process of an Fe ion. In short, the number of the interacting molecules effectively decreases due to the overlapping region. The reduced molecular number suppresses the change of the configuration entropy induced by the reduction process of an Fe ion. Thus, the overlap suppresses α ($= \frac{\Delta S}{e}$), in large m region.

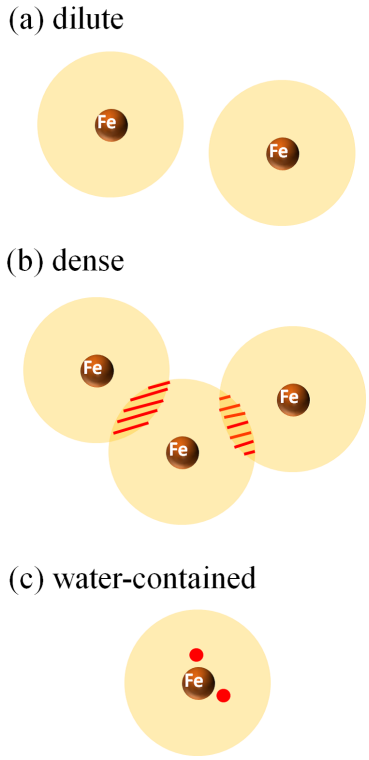

Fig. 4. (Color online) Schematic illustration of Fe ions in (a) dilute, (b) dense, and (c) water-contained solutions. Large circles represent the interaction area where solvent molecules interact with the Fe ion. Hatchings in (b) represent the overlap of the interaction areas. Small circles in (c) represent H_2O and/or OH^-.

3.3 Enhancement of α with m in protic solvent

Now, let us discuss the origin for the enhancement of α with m observed in protic solvents [Fig. 3(a)]. The electrolyte, $Fe(ClO_4)_2{\cdot}6H_2O/Fe(ClO_4)_3{\cdot}7.1H_2O$, used in the present investigation contains crystal water, and hence, the prepared electrolyte solutions contain some water. The water content in solution increases with m. For example, amount of water in Me solution is 2.9 wt% at 0.1 M and 8.2 wt% at 0.3 M. Fig. 5(a) shows the ΔT - V_0 plots of Me (circles) and Et (squares) at 0.1 M. Open and filled symbols represent the data with and without 5 wt% additional water. In Me (circles), addition of 5 wt% water enhances α from 1.18 mV/K to 1.50 mV/K. In Et (squares), addition of 5 wt% water enhances α from 0.82 mV/K to 1.27 mV/K. Thus, the water in solute is the origin for the enhanced α.

How does the water affect α? It is well known that Fe^{3+} ions in aqueous solution (pH < 4) is coordinated by OH^- and H_2O to form $[Fe(OH)(H_2O)_5]^{2+}$ monomer and/or $[Fe_2(OH)_2(H_2O)_8]^{4+}$ dimer.[40–43] The $[Fe(OH)(H_2O)_5]^{2+}$ monomer complex dominates in dilute ($\leq$ 1 mM) solution while the $[Fe_2(OH)_2(H_2O)_8]^{4+}$ dimer complex does in dense ($\geq$ 100 mM) solution. The monomer[42] shows a weak absorption at 300 nm while the dimer[40] shows

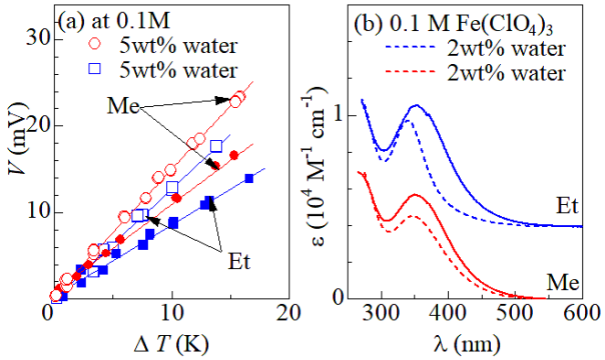

Fig. 5. (Color online) (a) V_0 against ΔT of Me (circles) and Et (squares) containing 0.1 M $Fe(ClO_4)_2{\cdot}6H_2O$ and 0.1 M $Fe(ClO_4)_3{\cdot}7.1H_2O$. Open and filled symbols represent the data with and without 5 wt% additional water, respectively. Straight lines are results of least-squares fitting. (b) Molar absorption coefficient (ϵ) spectra of 0.1 M $Fe(ClO_4)_3{\cdot}7.1H_2O$ dissolved in Me and Et. Solid and broken curves are the spectra with and without 2 wt% additional water, respectively.

a weak absorption at 340 nm. We observed the 340 nm absorption bands in the ultra violet-visible (UV-vis) absorption spectra of aqueous solutions containing 0.1 M $Fe(ClO_4)_3{\cdot}7.1H_2O$. The physical and chemical properties of protic solvents are similar to those of water. Then, if there exists a certain amount of water in protic solvent containing Fe^{3+}, it is possible for OH^- and/or H_2O to coordinate to Fe^{3+} as in aqueous solution.

The UV-vis absorption spectroscopy is a powerful tool to investigated the coordination state around Fe^{3+}, because it exhibits characteristic ligand-to-metal charge transfer (LMCT) transition. To investigate the effect of the water on the coordination state around Fe^{3+}, we carefully investigated the UV-vis absorption spectra of Me and Et solutions containing 0.1 M $Fe(ClO_4)_3{\cdot}7.1H_2O$ with and without of 2 wt% additional water. The UV-vis spectra were measured in a 0.1 mm quartz cell with a spectrometer (V750, Jasso) at room temperature. The molar absorption coefficient (ϵ) is expressed as $-\frac{1}{cd}\ln T$, where c (= 0.1 M) and d (= 0.1mm), and T are the concentration, optical path length, and transmittance spectrum, respectively. Figure 5(b) shows the ϵ spectra of Me and Et containing 0.1 M $Fe(ClO_4)_3{\cdot}7.1H_2O$. Solid and broken curves are the spectra with and without 2 wt% additional water, respectively. In the Me solution, the ϵ spectra (solid curve) without additional water shows an intense absorption band around 350 nm. The absorption band can be ascribed to the LMCT transition from the coordinated Me molecules to Fe $3d_{t2g}$ orbital. The addition of 2 wt% water (broken curve) significantly suppresses the LMCT band. The suppression suggests that part of the Fe^{3+} ions are coordinated by OH^- and/or H_2O, because such a coordination weakens and/or shift the

LMCT band. Actually, the monomer[42] shows a weak and broad absorption at 300 nm. A similar suppression of the LMCT band is observed in the ϵ spectra of the Et solution. In the Et solution, the additional water causes apparent peak shift to the low wavelength side. A careful comparison between the ϵ spectra of the water-added Me and Et solutions reveals that the spectrum of the Et solution has a intense absorption component at 340 nm. The component implies that dimers are formed in the water-added Et solutions, bacause the dimer[40] shows a rather sharp absorption band at 340 nm.

Figure 4(c) schematically shows the Fe ion in water-contained solution. The reduction process of the central Fe ion changes the configuration entropy of the solvent molecules in the interaction area (large circles), which is the main origin for ΔS in a solute-solvent system. Small circles in (c) represent H_2O and/or OH^-, which coordinates to the Fe ion. The configurational entropy in the interaction area is considered to enhance by partial replacement of the coordinated solvent molecules with H_2O and/or OH^-, because the mixing of the different kinds of interaction, *i.e.*, the solvent-solvent, H_2O-solvent, and OH^--solvent interactions, causes a variety of energetically degenerate local structures around the Fe complex. Thus, the heterologous coordination enhances ΔS, and hence α ($= \frac{\Delta S}{e}$), in small m region. Actually, the α value (= 1.85 mV/K at 0.5 M) in the water-contained Me is higher than the values in pure water (= 1.56 mV/K[1] at 0.5 M) and pure Me ($\approx$ 1.0 mV/K at $m \rightarrow 0$ M). Similarly, the α value (= 1.78 mV/K at 0.5 M) in the water-contained Et is higher than the values in pure water (= 1.56 mV/K[1] at 0.5 M) and pure Me ($\approx$ 0.6 mV/K at $m \rightarrow 0$ M).

The α values in protic solvents increase with m in small m region and decrease with m in large m region [Fig. 3(a)]. As discussed above, the enhancement of α in small m region is ascribed to the heterologous coordination to the Fe ion. The effect of the heterologous coordination is suppressed in large m region where the Fe ion is coordinated mainly by H_2O and OH^-. In addition, the overlap of the interaction area suppresses α in the large m region, as discussed in the previous subsection. Due to the competition between the enhancement and suppression effects on α, α shows maximum value at intermediate m.

3.4 I - V plot

Figure 6 shows I - V plot in LTEs composed of (a) Me, (b) Et, (c) Pr, (d) EG, (e) THF, (f) PC, (g) DMF, and (h) DMSO. ΔT was fixed at 30 K. In (a) Me LTE, V linearly decreases with I, as indicated by straight lines. The slope is proportional to the reciprocal of - σ. A similar linear relation in the $I - V$ plot is observed in whole the LTEs investigated [Fig. 6(b) - (h)]. In (a) Me LTE, the σ value increases from 17.9 mS/cm at 0.1 M to 33.9 mS/cm at 0.5 M, and

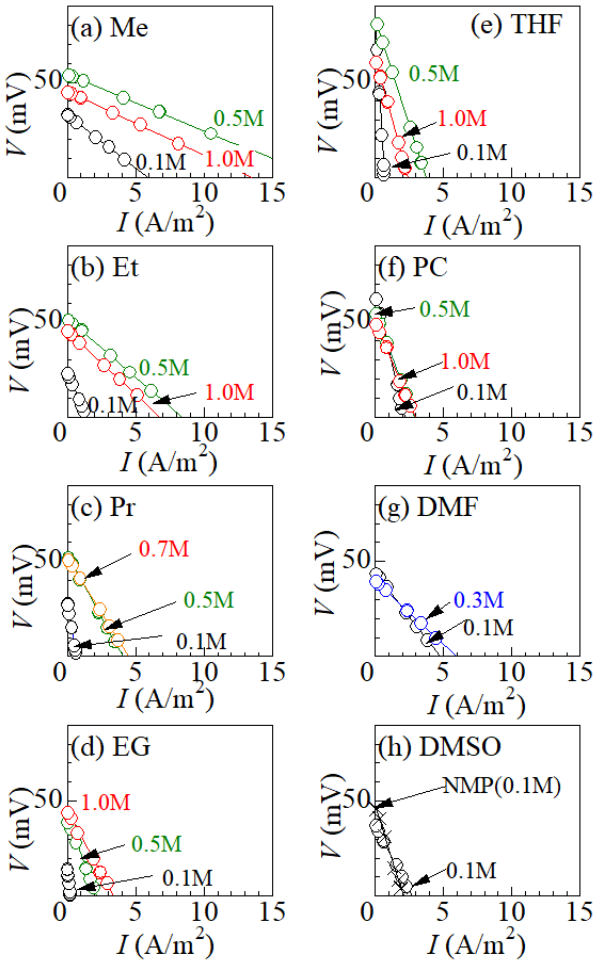

Fig. 6. (Color online) I - V plot os LTEs composed of (a) Me, (b) Et, (c) Pr, (d) EG, (e) THF, (f) PC, (g) DMF, and (h) DMSO containing m M $Fe(ClO_4)_2 \cdot 6H_2O$ and m M $Fe(ClO_4)_3 \cdot 7.1H_2O$. ΔT was fixed at 30 K. Straight lines are results of least-squares fitting.

then, decreases to 14.9 mS/cm at 1.0 M. In (e) THF LTE, the σ value increases from 0.81 mS/cm at 0.1 M to 4.5 mS/cm at 0.5 M, and then, decreases to 3.7 mS/cm at 1.0 M.

Figure 7 shows m-dependence of σ in (a) protic and (b) aprotic solvents. In the Me LTE, the σ value increases with m in the small m region from 17.9 mS/cm at 0.1 M to 36.4 mS/cm at 0.7 M. The increase in σ is originated in the increase in the density of carriers or Fe ions. A similar increase in σ is observed in the LTEs composed of the other eight solvents. In the Me LTE, the σ value decreases with m in the large m region. Such a decrease in σ is probably ascribed to the interaction among the carriers or Fe ions. Another limiting factor for σ is the redox reaction at the electrode-electrolyte interface. For a steady redox reaction to occur, the ionic species oxidized/reduced at the electrode must quickly escape from the vicinity of the electrode. In the large m region, concentration overpotential effect[44] or accumulation of

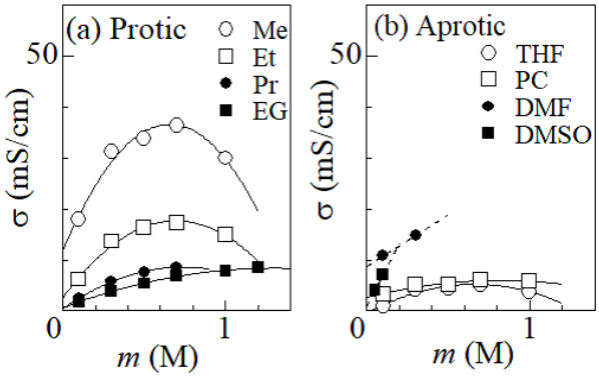

Fig. 7. Electric conductivity (σ) of (a) protic and (b) aprotic solvents against electrolyte concentration (m). Solid curves are results of least-squares fitting with quadratic functions. Broken straight lines in (b) are results of least-squares fitting.

Table I. Parameters of LTEs composed of several solvents containing m M $Fe(ClO_4)_2{\cdot}6H_2O$ and m M $Fe(ClO_4)_3{\cdot}7.1H_2O$. α_{max}, σ_{max}, PF_{max}, m_{max} are the maximum values of electrochemical Seebeck coefficient, electric conductivity, power factor, and concentration, respectively. ΔT was fixed at 30 K. κ is the thermal conductivity of solvent without solutes and is cited from literature.[45] Me, Et, Pr, EG, THF, PC, DMF. DMSO, NMP. and AN stand for methanol, ethanol, 1-propanol, ethylene glycol, tetrahydrofuran, propylene carbonate, N,N-dimethylformamide, and dimethyl sulfoxide, N-methyl pyrrolidone, and acetonitrile, respectively.

solvent	α_{max} (mV/K)	σ_{max} (mS/cm)	κ (W/Km)	PF_{max} (μW/K^{2}m)	m_{max} (M)	
Me	1.85@0.5 M	36.4@0.7M	0.200	11.5@0.5M	≥2.0	this work
Et	1.78@0.5 M	17.2@0.7M	0.163	5.1@0.5M	1.5	this work
Pr	1.78@0.5 M	8.6@0.7M	0.149	2.5@0.7M	0.8	this work
EG	1.51@0.7 M	8.5@1.2M	0.256	1.9@1.2M	≥1.5	this work
THF	3.16@0.1 M	5.1@0.7M	0.153	4.1@0.7M	1.2	this work
PC	2.32@0.1 M	5.9@0.7M	0.164	2.0@0.7M	≥1.5	this work
DMF	1.49@0.1 M	14.8@0.3M	0.184	2.5@0.1M	0.3	this work
DMSO	1.38@0.05M	7.1@0.1M	0.186	1.2@0.1M	0.1	this work
NMP	1.57@0.1 M	4.3@0.1M	0.167	1.1@0.5M	0.1	this work
water	1.56@0.5 M	95.7@0.5M	0.597	23.1@0.5M	≥2.0	Ref.[1]
acetone	2.88@0.1 M	15.1@0.7M	0.155	8.5@0.5M	1.2	Ref.[1]
AN	2.83@0.1 M	21.1@0.5M	0.199	9.6@0.5M	0.8	Ref.[1]

oxidized/reduced ionic species in the vicinity of electrode becomes significant. Such an effect suppresses σ during the device operation. A similar decrease in σ is clearly observed in the Et and THF LTEs. In the Pr, EG, and PC LTEs, the increase in σ saturates in the large m region.

3.5 Solvent dependence of LTE performance

In Table I, we summarized parameters of LTEs composed of several solvents. ΔT was fixed at 30 K. α_{max}, σ_{max}, PF_{max}, m_{max} are the maximum values of α, σ, PF, and m, respectively. PF_{max} of the Me LTE is 11.5 $\mu W/K^2m$ at 0.7 M. The high PF_{max} value of the Me LTE is ascribed to moderate α and large σ. Importantly, the α value increases with m in protic solvents [Fig. 7(a)]. The enhancement of α is essential for realizing high PF_{max} because α and σ can be maximized at similar m value. The α and σ values in the Me LTE take maxima at 0.5 and 0.7 M, respectively (Table I). The Et LTE shows the second highest PF_{max} (= 5.1 $\mu W/K^2m$ at 0.5 M) among the nine organic LTEs investigated, reflecting moderate α and large σ.

The THF LTE shows the highest α_{max} (= 3.16 mV/K at 0.1 M) among the nine organic LTEs investigated, reflecting weak interaction between the solute ion and solvent molecule. A disadvantage of aprotic solvents, however, is small σ. σ_{max} of the THF LTE is 5.1 mS/cm at 0.1 M. As a results, PF_{max} (= 4.1 $\mu W/K^2m$ at 0.7 M) of the THF LTE is much lower than PF_{max} (= 11.5 $\mu W/K^2m$ at 0.7 M) of the Me LTE. The PC LTE shows the second highest α_{max} (= 2.32 mV/K at 0.1 M) among the nine organic LTEs investigated. However, ZT_{max} (= 2.0 $\mu W/K^2m$ at 0.7 M) of the PC LTE is much lower than PF_{max} of the Me LTE.

The maximum values (ZT_{max}) of ZT is expressed as $\frac{TPF_{max}}{\kappa}$. In order to accurately evaluate the ZT_{max}, it is necessary to know the κ value during the LTE operation. We note that κ may depend on m similarly to the case of α and σ. In addition, the convection in the operating LTE may influence κ due to the enhanced mass transport. At present, we do not know the exact value of κ during the LTE operation. We tentatively evaluate ZT_{max} with κ of solvents without solutes.[45] ZT_{max} of the Me LTE is 0.0172 at 0.7 M, which is larger than ZT_{max} (= 0.0116[1] at 0.5 M) of the corresponding aqueous LTE, reflecting small κ (= 0.200 W/Km). The Et LTE shows the second highest ZT_{max} (= 0.094 at 0.5 M) among the nine organic LTEs investigated, reflecting small κ (= 0.163 W/Km).

4. Conclusion

In conclusion, we evaluated the performances of LTEs composed of nine organic solvent containing Fe^{2+}/Fe^{3+} redox pair against m. At ΔT = 30 K, ZT_{max} of the Me LTE is 0.0172 at 0.7 M, which is larger than ZT_{max} (= 0.0116 at 0.5 M) of the corresponding aqueous LTE. In protic solvents, the α value increase with m in small m region due to the crystal water in the solute. The enhancement of α is interpreted in terms of the heterologous coordination to the Fe ion.

Acknowledgments

This work was supported by JSPS KAKENHI (Grant Numbers 22J11837), Murata Science Foundation, and joint research with Taisei Rotec Corporation.

References

1) A. Wake, D. Inoue, and Y. Moritomo, Appl. Phys. Express **15**, 054002 (2022).
2) T. Ikeshoji, Bull Chem. Soc. Jpn. **60**, 1505 (1987).
3) T. Kim, J. S. Lee, G. Lee, H. Yoon, J. Yoon, T. J. Kangd, and Y. H. Kim, Nano Energy **31**, 160 (2017).
4) H. Zhou, T. Yamada, and N. Kimizuka, J. Am. Chem. Soc. **138**, 10502 (2016).
5) I. Quickenden, and Y. Mua, J. Electrochem. Soc. **142**, 3985 (1995).
6) Y. Mua, and T. I. Quickenden, J. Electrochem. Soc. **143**, 2558 (1996).
7) D. R. MacFarlane, N. Tachikawa, M. Forsyth, J. M. Pringle, P. C. Howlett, G. D. Elliott, J. F. Davis, Jr., M. Watanabe, P. Simon, and C. A. Angell, Energy Environ. Sci. **7**, 232 (2014).
8) M. Bonetti, S. Nakamae, M. Roger, and P. Guenoun, J. Chem. Phys. **134**, 114513 (2011).
9) N. Jiao, T. J. Abraham, D. R. MacFarlane, and J. M. Pringle, J. Electrochem. Soc. **161**, D3061 (2014).
10) J. Kawamura, M. Shimoji, and H. Hoshino, J. Phys. Soc. Jpn. **50**, 194 (1981).
11) A. Schiraldi, E. Pezzati, and P. Baldini, J. Phys. Chem. **89**, 1528 (1985).
12) J. Duan, G. Feng, B. Yu, J. Li, M. Chen, P. Yang, J. Feng, K. Liu, and J. Zhou, Nat Commun. **9**, 5146 (2018).
13) M Sindhuja, B Lohith, V Sudha, G R Manjunath, and S Harinipriya Mater. Res. Express **4**, 075513 (2017).
14) A. Gunawan, C.-H. Lin, D. A. Buttry, V. Mujica, R. A. Taylor, R.S. Prasher, and P. E. Phelan, Nanoscale Microsc. Thermophys. Eng. **17**, 304 (2013).
15) A. Gunawan, H. Li, C.-H. Lin, D. A. Buttry, V. Mujica, R.A. Taylor, R.S. Prasher, and P. E. Phelan, Int. J. Heat Mass Trans. **78**, 423 (2014).
16) R. Hu, B.A. Cola, N. Haram, J.N. Barisci, S. Lee, S. Stoughton, G. Wallace, C. Too,M. Thomas, A. Gestos, M.Ed Cruz, J.P. Ferraris, A.A. Zakhidov, and R.H. Baughman, Nano Lett. **10**, 838 (2010).
17) M. Romano, S. Gambhir, J. Razal, A. Gestos, and G. Wallace, J. Chen, J. Therm. Anal Calorim. **109**, 1229 (2012).
18) M. S. Romano, N. Li, D. Antiohos, J. M. Razal, A. Nattestad, S. Beirne, S. Fang, Y. Chen, R. Jalili, G. G. Wallace, and R. Baughman, J. Chen, Adv. Mater. **25**, 6602 (2013).
19) T. J. Abraham, D. R. MacFarlane, and J. M. Pringle, Energy Environ. Sci. **6**, 2639 (2013).

20) T. J. Abraham, D. R. MacFarlane, and J. M. Pringle, Chem. Commun. **47**, 6260 (2011).
21) M. A. Lazar, D. Al-Masri, D. R. MacFarlane, and J. M. Pringle, Phys. Chem. Chem. Phys. **18**, 1404 (2016).
22) H. Im, T. Kim, H. Song, J. Choi, J. S. Park, R. Ovalle-Robles, H. D. Yang, K. D. Kihm, R. H. Baughman, H. H. Lee, T. J. Kang, and Y. H. Kim, Nat. Commun. **7**, 10600 (2016).
23) S. W. Lee, Y. Yang, H.-W. Lee, H. Ghasemi, D. Kraemer, G. Chen, and Y. Cui, Nat. Commun. **5**, 3942 (2014).
24) Y. Yang, J. Loomis, H. Ghasemi, S. W. Lee, Y.J. Wang, Y. Cui, and G. Chen, Nano Lett.**14**, 6578 (2014).
25) Y. Yang, S. W. Lee, H. Ghasemi, J. Loomis, X. Li, D. Kraemer, G. Zheng, Y. Cui, and G. Chen, Proc. Natl. Acad. Sci. USA **111**, 17011 (2014).
26) A. Hartel, M. Janssen, D. Weingarth, V. Presser, and R. van Roij, Energy Environ. Sci. **8**, 2396 (2015).
27) R. Long, B. Li, Z. Liu, and W. Liu, Energy **87**, 463 (2015).
28) R. Long, B. Li, Z. Liu, and W. Liu, Energy **107**, 95 (2016).
29) P. F. Salazar, S. Kumar, and B. A. Cola, J. Electrochem. Soc. **159**, B483 (2012).
30) S. Uhl, E. Laux, T. Journot, L. Jeandupeux, J. Charmet, and H. Keppner, J. Electron. Mater. **43**, 3758 (2014).
31) A. H. Kazim, and B. A. Cola, J. Electrochem. Soc. **163**, F867 (2016).
32) H. J. Goldsmid, *Introduction to Thermoelectricity* (Springer, Berlin, 2010).
33) M. A. Buckingham, F. Marken, and L. Aldous, Susten. Ener. Fuel, **2**, 2717 (2018).
34) J. H. Kim, J. H. Lee, R. R. Palem., M.-S. Suh, H. H. Lee, and T. J. Kang, Sci. Reps. **9**, 8706 (2019).
35) D. Inoue, H. Niwa, H. Nitani, and Y. Moritomo, J. Phys. Soc. Jpn. **90**, 033602 (2021).
36) Y. Fukuzumi, Y. Hinuma, and Y. Moritomo, Jpn. J. Appl. Phys. **58**, 065501 (2019).
37) P. F. Salazar, S. Kumar, and B. A. Cola, J Appl Electrochem. **44**, 325 (2014).
38) Y. Mua, and T. I. Quickenden, J. Electrochem. Soc. **143**, 2558 (1996).
39) J. N. Israelashvili, *Intermolecular and surface forces* (Elsevier, California, 2014).
40) L. N. Mulay and P. W. Selwood, J. Am. Chem. Soc. 77, 2693 (1955)
41) R. J. Night and R. N. Sylva, J. Inorg. Nucl. Chem. 37, 779 (1975).
42) H.-J. Benkelberg and Peter Warneck, J. Phys. Chem. 99, 5214 (1995).
43) R. A. Danforth and B. Kohler, Chem. Phys. Lett. 683, 315 (2017).
44) P. F. Salazar, S. Kumar, B. A. Cola, J. Appl. Electrochem. 44, 325 (2014).
45) J. R. Rumbel, ed., *CRC Handbook of Chemistry and Physics*, 102nd Ed., (CRC press,

Boca Ranton, 2021).